Biophysical Journal Volume 108 April 2015 2038–2047

Article

# Direct Detection of α-Synuclein Dimerization Dynamics: Single-Molecule Fluorescence Analysis

Zhengjian Lv,[1] Alexey V. Krasnoslobodtsev,[1] Yuliang Zhang,[1] Daniel Ysselstein,[2] Jean-Christophe Rochet,[2] Scott C. Blanchard,[3,4] and Yuri L. Lyubchenko[1,*]

[1]Department of Pharmaceutical Sciences, University of Nebraska Medical Center, Omaha, Nebraska; [2]Department of Medicinal Chemistry and Molecular Pharmacology, Purdue University, West Lafayette, Indiana; [3]Department of Physiology and Biophysics, Weill Cornell Medical College, New York, New York; and [4]Tri-Institutional Training Program in Chemical Biology, Weill Cornell Medical College, and Rockefeller University, and Memorial Sloan-Kettering Cancer Center, New York, New York

ABSTRACT The aggregation of α-synuclein (α-Syn) is linked to Parkinson's disease. The mechanism of early aggregation steps and the effect of pathogenic single-point mutations remain elusive. We report here a single-molecule fluorescence study of α-Syn dimerization and the effect of mutations. Specific interactions between tethered fluorophore-free α-Syn monomers on a substrate and fluorophore-labeled monomers diffusing freely in solution were observed using total internal reflection fluorescence microscopy. The results showed that wild-type (WT) α-Syn dimers adopt two types of dimers. The lifetimes of type 1 and type 2 dimers were determined to be 197 ± 3 ms and 3334 ± 145 ms, respectively. All three of the mutations used, A30P, E46K, and A53T, increased the lifetime of type 1 dimer and enhanced the relative population of type 2 dimer, with type 1 dimer constituting the major fraction. The kinetic stability of type 1 dimers (expressed in terms of lifetime) followed the order A30P (693 ± 14 ms) > E46K (292 ± 5 ms) > A53T (226 ± 6 ms) > WT (197 ± 3 ms). Type 2 dimers, which are more stable, had lifetimes in the range of several seconds. The strongest effect, observed for the A30P mutant, resulted in a lifetime 3.5 times higher than observed for the WT type 1 dimer. This mutation also doubled the relative fraction of type 2 dimer. These data show that single-point mutations promote dimerization, and they suggest that the structural heterogeneity of α-Syn dimers could lead to different aggregation pathways.

## INTRODUCTION

Self-assembly of protein into amyloid-type aggregates is a widespread phenomenon associated with the development of many neurodegenerative diseases, including Parkinson's disease (PD), a hallmark of which is the aggregation of α-synuclein (α-Syn) and the assembly of aggregates into intracellular Lewy bodies (1,2). Amyloid self-assembly kinetics are described by a nucleation and growth mechanism in which the first phase, nucleation, produces a critical oligomer that gives rise to the second phase, a thermodynamically favorable elongation process, resulting in the formation of fibrillary aggregates (3). Biophysical techniques have been applied in the structural characterization of amyloid or amyloid-like fibrils, revealing a number of general features of aggregates formed by the assembly of amyloid proteins, including α-Syn (4–7).

α-Syn is a relatively small protein comprised of 140 residues that belongs to the family of intrinsically disordered proteins (IDPs). In aqueous solution, the protein lacks clear structural motifs and is characterized by a globular shape slightly smaller than a random coil (6,7). In fibrils, however, α-Syn undergoes a dramatic structural transition involving the formation of β-sheet structural motifs that primarily span the central hydrophobic part of the protein, referred to as the nonamyloid component (NAC, amino acids 61–95). Dramatic conformational transitions of this nature typify fibrils formed by IDPs, whereas structurally organized amyloid proteins (e.g., Sup35 prion protein) can form fibrils without undergoing such a dramatic structural change (7). The key common feature of amyloid-like fibrils is an extended β-sheet that stabilizes the fibrillar structure (8,9). The conversion of amyloidogenic proteins to β-sheet-rich assemblies involves a dramatic change in the protein conformation that has been termed protein misfolding.

Compared to our understanding of the elongation process, knowledge of the first phase of α-Syn self-assembly, the formation of oligomers, is limited due to the lack of appropriate techniques to characterize temporal features of the assembly process. Oligomeric states of the protein are transient, so their characterization requires nontraditional approaches. Single-molecule techniques are capable of characterizing transient states of amyloid proteins (reviewed in (10,11)). Sandal et al. applied atomic-force-microscopy (AFM)-based single-molecule force spectroscopy (SMFS) to characterize conformational equilibria of α-Syn monomers (12). A number of environmental factors and pathogenic mutations known to promote α-Syn aggregation were found to shift the equilibria to structured conformers (13). The

*Submitted November 10, 2014, and accepted for publication March 9, 2015.*

*Correspondence: ylyubchenko@unmc.edu

Editor: Ashok Deniz.



0006-3495/15/04/2038/10 $2.00

http://dx.doi.org/10.1016/j.bpj.2015.03.010

same method was adopted by Hervás et al. to reveal a conformational polymorphism of monomeric forms of amyloidogenic proteins, including α-Syn (14). Optical tweezers methods were applied to identify a range of metastable structures for α-Syn monomers, dimers, and tetramers (15). Trexler and Rhoades utilized single-pair Förster resonance energy transfer to explore the aggregation-prone states of α-Syn monomer (16), revealing an important role of the C-terminus. Single-molecule Förster resonance energy transfer was also used to demonstrate the structural transition between the broken horseshoe and the extended α-helix structures of α-Syn upon binding to lipids (17). Based on our understanding of α-Syn fibrillar structure, discussed above, it is widely assumed that the aggregation of α-Syn and other amyloid proteins is initiated by the formation of misfolded monomers and their assembly into dimers. The monomer structure changes upon interaction with an oligomer, and a detailed computational model of this process, termed dock and lock, has recently been developed (18). In that model, the unstructured monomer, after docking to the structured oligomer, adopts a conformation required to lock the oligomer, adding one more unit to the structured assembly.

Recently, our group developed an AFM-based SMFS approach designed to monitor the interaction between monomers tethered to the surface and the AFM tip (11,19–28). Using this approach, misfolded states of α-Syn and other proteins have been probed to reveal a number of common features. For example, we showed that dimers with different conformations form, and we identified protein segments involved in the interprotein interaction. In addition, the dimers were shown to be stable and characterized by lifetimes in the range of 1 s.

The application of the SMFS approach to amyloid β (Aβ) proteins revealed dramatic differences in folding pattern between the Aβ40 and Aβ42 dimers, and the N-terminal segment of the protein was found to play a critical role in the protein folding (26). Probing of α-Syn interactions enabled us to identify α-Syn segments involved in dimer assembly and to characterize the impact of familial mutations of α-Syn on the misfolded dimer conformations (24). Evidence that misfolded dimers exhibit high stability led to the hypothesis that the formation of such dimers is the mechanism by which the misfolded state of amyloidogenic proteins is stabilized, suggesting that dimerization triggers the self-assembly process (11). Recent computational analyses confirmed this hypothesis (29). Molecular dynamics (MD) simulations played an important role in demonstrating that misfolded conformations did not occur in monomers but did appear in dimers, which remained stable over timescales of several hundreds of nanoseconds, whereas monomers changed their conformations in a few nanoseconds. In addition, these studies revealed a set of misfolded dimeric conformations, which led to our hypothesis that various dimeric conformers are involved in the amyloid oligomerization process. Although there is a nice qualitative correlation between the high stability of dimers measured by SMFS and that obtained in MD simulations, the dimers in the experiment were probed along the applied force, so the impact of dimer fluctuations in other directions on dimer stability remains unclear. We address that issue in this study, in which a single-molecule fluorescence approach was developed to probe dimer stability.

Here, we applied single-molecule fluorescence imaging to measure directly the lifetimes of α-Syn dimers. In this approach, unlabeled α-Syn was tethered to the coverslips, and fluorescently labeled α-Syn in the solution was capable of interacting with the immobilized α-Syn to form dimers. Dimer formation was detected by fluorescence bursts, and dimer lifetimes were quantified. Statistical analysis revealed long-lived dimers, with lifetimes exceeding hundreds of milliseconds. In particular, we identified two major populations of such dimers with lifetimes of several hundreds of milliseconds and several seconds, whose lifetimes and relative distributions were altered by specific disease-related mutations.

## MATERIALS AND METHODS

### Materials

Phosphate-buffered saline (PBS), pH 7.0, was prepared and filtered through a disposable Millex-GP syringe filter unit (0.22 μm) before use. All reagents were purchased from Sigma Aldrich (St. Louis, MO). In all experiments, we used square glass coverslips (20 mm × 20 mm; Karl Hecht, Sondheim, Germany), potassium dichromate (ICN Biomedicals, Aurora, OH), and deionized (DI) water (18.2 MΩ resistivity, 0.22 μm filter pore size; APS Water Services, Van Nuys, CA). A stock solution of 50 mM 1-(3-aminopropyl) silatrane (APS) was prepared by dissolving the APS powder in DI water. The intramolecularly photostabilized Cy3 fluorophore (GE Healthcare, Little Chalfont, United Kingdom) was chemically synthesized (30). Maleimide-poly(ethylene glycol)-succinimidyl valerate (Mal-PEG-SVA, 3.4 kDa), SVA-PEG-SVA, and methoxy-PEG-SVA (mPEG-SVA, 2 KDa) were purchased from Laysan Bio (Arab, AL). In addition, we used sodium bicarbonate (Mallinckrodt Baker, Paris, KY), Amicon 10 kDa and 30 KDa centrifugal filter units (EMD Millipore. Billerica, MA), mica sheets (Asheville-Schoonmaker Mica, Newport News, VA), carbon-coated double-sided tape (Ted Pella, Redding, CA), and 0.1-mm-thick teflon spacers (American Durafilm, Holliston, MA). All α-Syn proteins were prepared as described in our previous publications (22,24), and details are provided in the Supporting Material.

### Total internal reflection fluorescence microscopy imaging

Glass coverslips were cleaned with potassium dichromate for 30 min and immersed in DI water until use. Glass coverslips were assembled on the original sample holder (PicoQuant, Berlin, Germany), then covered by a 0.1-mm-thick teflon spacer and a 25-mm-diameter quartz disk. The created sample chamber was then filled with an aqueous solution of 167 mM APS for 30 min and rinsed with DI water, resulting in a glass surface modified with primary amine groups. The APS coverslips were functionalized with a 1:100 Mal-PEG-SVA/mPEG-SVA molar mixture (31,32) by incubation for 1 h in 0.1 M sodium bicarbonate buffer, pH 8.5 (33). Bubbles were removed from the sodium bicarbonate buffer by vortexing and ultrasonication. The sample chamber was sequentially rinsed with sodium bicarbonate

buffer, pH 8.5, and 10 mM PBS buffer, pH 7.0, before immobilization of α-Syn. The α-Syn solution was sonicated (Branson 1210, Branson Ultrasonics, Danbury, CT) and then filtered through an Amicon filter (molecular weight cutoff, 30 kDa) at 14,000 rpm for 15 min to remove aggregates. For surface immobilization, the α-Syn solution (25 pM fluorescently labeled or unlabeled) was injected into the sample chamber to allow Cys moieties of α-Syn to react with maleimide groups of immobilized Mal-PEG-SVA during a 1 h incubation. The sample chamber was thoroughly rinsed with PBS buffer solution and used immediately.

Single-molecule imaging was performed with an objective-type total internal reflection fluorescence (TIRF) microscope built around an Olympus IX71 microscope (Hitschfel Instruments, St. Louis, MO). An oil-immersion UPlanSApo 100× objective with 1.40 NA (Olympus, Tokyo, Japan) was used for all measurements. A laser line at 532 nm (CrystaLaser, Reno, NV) was used to excite the fluorophore of immobilized α-Syn in the total internal reflection mode. Fluorescence emission was detected with an electron-multiplying charge-coupled-device camera (ImagEM Enhanced C9100-13, Hamamatsu, Bridgewater, NJ). TIRF videos of 45 s to 50 s duration were recorded at a temporal resolution of 30 ms. The labeled 1 nM α-Syn solution (labeling procedures can be found in the Supporting Material) was sonicated for 1 min to break aggregates and filtered through an Amicon filter (molecular weight cutoff, 30 kDa) at 14,000 rpm for 15 min. TIRF experiments were repeated three times for each protein.

Double cysteinyl α-Syn enabling fluorescence labeling and covalent immobilization was used in experiments in which the density of α-Syn surface coverage was adjusted. Before the surface immobilization, a 100 pM solution of Cy3 α-Syn was sonicated for 1 min to break aggregates and filtered through an Amicon filter (molecular weight cutoff, 30 kDa) at 14,000 rpm for 15 min. The filtered α-Syn solution was immobilized on the PEG-functionalized coverslips using the procedure described above. The experiments were repeated three times.

## TIRF data analysis

The videos recorded with TIRF were visually inspected frame by frame using Slidebook 5.0 software (Intelligent Imaging Innovations (3i), Denver, CO). Whenever a candidate dimer was detected, a confined area was circled out for further analysis. A typical dimerization event showed a sudden increase of fluorescence intensity with an abrupt drop back to background after a short time period. The increment threshold of fluorescence intensity was set at three times higher than the standard deviation of background fluctuation. Several hundreds of dimers were analyzed for each protein. The data were assembled and shown as a distribution.

The normalized survival probability, $P_{surv}$, was used to measure the lifetime of α-Syn dimers. A prominent characteristic of the NSP approach is that it does not require any assumptions about the type of data distribution (34,35). Therefore, if the decay process is complicated (e.g., multiexponential), the NSP approach is capable of extracting features for all species. $P_{surv}$ was calculated by dividing the number of events that fall into each time-bin interval by the total number of events. The original distribution of counts versus lifetime was transformed into another display in which $P_{surv}$ was plotted versus lifetime according to the equation

$$P_{surv} = \frac{n_{surv}(t)}{N}, \quad (1)$$

where $n_{surv}(t)$ is the number of dimerization events that survive longer than lifetime $t$, and $N$ is the total number of dimerization events detected. Compared with single- and triple- exponential decay (Table S1), the data were best fitted with a double-exponential decay process, which we ascribe to two types of dimers with distinct lifetimes, $\tau_1$ and $\tau_2$:

$$P_{surv}(t) = A_1 \times \exp\left(\frac{t}{\tau_1}\right) + A_2 \times \exp\left(\frac{t}{\tau_2}\right) \quad (2)$$

where $A_1$ and $A_2$ are fractions of species with lifetimes $\tau_1$ and $\tau_2$, respectively.

The Kolmogorov-Smirnov test (no assumption of data distribution required) was used to test the difference between the two identified distributions for each experiment.

The free energies were estimated according to methods in previous studies, using the equation (36)

$$\Delta G^{\#} = \ln\left(\frac{k_B T}{k_{off} \times h}\right) k_B T, \quad (3)$$

where $\Delta G^{\#}$ is the height of the energy barrier, $k_B$ is the Boltzmann constant, $T$ is temperature, $h$ is the Planck constant, and $k_{off}$ (the reciprocal value of $\tau_1$ and $\tau_2$) is the dissociation rate without applied external force.

Single-molecule fluorescence traces of covalently immobilized α-Syn were manually selected for analysis. The number of photobleaching steps in each trace was determined according to published procedures (37). All fluorescence traces contained only one or two bleaching steps. At least 100 molecules were analyzed for each sample.

# RESULTS

## Tethered approach outline

We designed the approach for direct visualization of α-Syn interactions at the single-molecule level using single-molecule fluorescence in the TIRF mode. In this approach, schematically shown in Fig. 1, α-Syn proteins (wild-type (WT) and three mutants, A30P, E46K, and A53T (Fig. 1 *A*)) are immobilized on a coverslip and allowed to interact with fluorescently labeled α-Syn in the solution to form a complex

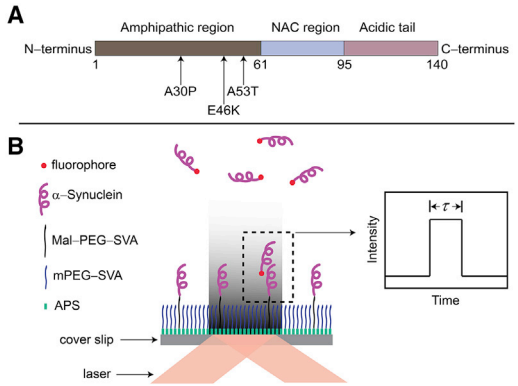


FIGURE 1 (*A*) Schematic of the structure of α-Syn. The amphipathic region (1–61), nonamyloid component region (NAC, 61–95), and acidic tail (95–140) are colored dark gray, light blue, and light pink, respectively. Arrows indicate the three single-point mutations, A30P, E46K, and A53T. A cysteine is tagged at the C-terminus for single cysteinyl α-Syn. Two cysteines are placed at both ends for double cysteinyl α-Syn. (*B*) Schematic of the TIRF setup. A glass coverslip is functionalized with APS, followed by functionalization with two types of PEG and immobilization of the unlabeled α-Syn. The solution of the labeled α-Syn (shown with red dots at one end) is injected into the sample chamber, allowing free α-Syn molecules to interact with the tethered protein molecules. A laser is brought to the sample in the total internal reflection mode, enabling the generation of an evanescent field and excitation of molecules in the proximity of the surface. The dimerization event is detected by the appearance of a fluorescence burst with duration $\tau$ defining the dimer lifetime, as shown schematically (*inset*). To see this figure in color, go online.

(dimer). Dimer formation is detected by the appearance of a fluorescence burst at the location of the transiently formed dimer (Fig. 1 *B*). The duration of the burst is the measure of the α-Syn dimer lifetime. To minimize the effect of α-Syn immobilization on the interaction with free protein molecules, α-Syn molecules were tethered to the surface via flexible PEG linkers. We used bifunctional PEG tethers that were covalently immobilized on the amino-modified surface (i.e., the APS surface) (27) via the reaction of the SVA terminal reactive group (the N-hydroxysuccinimide group) making the maleimide terminus (Mal group) of immobilized PEG available for reaction with the thiol group of the α-Syn cysteine residue. α-Syn does not contain cysteine residues, so we used an A140C derivative of α-Syn in which the C-terminal alanine was replaced with cysteine. The rationale for using the C-terminal domain for α-Syn immobilization stems from the well-documented fact that the C-terminal segment of α-Syn is not involved in protein aggregation; therefore, C-terminal immobilization via cysteine provides the fewest potential constraints for the interaction of immobilized α-Syn with free protein. Indeed, a similar immobilization of α-Syn was used in our prior AFM force spectroscopy studies, in which the interactions between two immobilized α-Syn proteins were probed (11,19,22,24). The same terminal cysteine was used for fluorescence labeling of α-Syn that was free in solution in the experimental setup (Fig. 1 *B*). A number of critical issues have to be addressed to accomplish the experiments as described in the scheme (Fig. 1 *B*).

First, the duration of the dye fluorescence should be long enough to enable us to measure the dimer lifetime before fluorophore bleaching. To ensure slow photobleaching, we used organic fluorophores that were photostabilized through intramolecular triplet-state quenching (38). We tested the stability of a given fluorophore conjugated to α-Syn in experiments in which labeled α-Syn was covalently immobilized on the PEG-ylated surface. In these experiments, α-Syn containing two cysteines (one each at the N- and C-termini) was used. One Cys residue enabled the conjugation of the dye, whereas the other provided immobilization of Cy3-labeled molecules to the glass coverslips functionalized with PEG-maleimide. There was no blinking or bleaching of the fluorescence spots during the observation time (see Movie S1 and the time trajectory shown in Fig. S1). Thus, these data directly confirmed the fluorescence stability of the label within the protein and under the environmental conditions used for these experiments. Second, the surface coverage of α-Syn should be sparse, to avoid overlap of fluorescence signals from labeled α-Syn bound to two adjacent immobilized α-Syn molecules. This criterion was met by adjusting the surface density of PEG-maleimide and the α-Syn concentration. The surface density of PEG-maleimide was controlled by the use of an excess of mPEG-SVA along with the main tether, Mal-PEG-SVA, both of which bind covalently to amines of the APS-glass surface. Because mPEG-SVA does not have a reactive maleimide group, the ratio between the two PEG tethers allowed us to adjust the surface density of these groups as needed for α-Syn immobilization. The conditions for the surface preparation and α-Syn concentration were identified by experiments with the use of Cy3-labeled α-Syn that contained two cysteines at the N- and C-termini, as described above. Fig. S2 *A* shows that individual bright spots were well separated with the distance (approximately microns) between the adjacent spots. Third, we tested the level of nonspecific binding of α-Syn. The experiments using the mPEG-SVA surface showed that the level of binding of Cy3-labeled α-Syn is very low (cf. Fig. S2, *A* and *B*). Nonspecific adsorption of dyes on other surfaces was also tested (Fig. S3). Fourth, we ensured that immobilized Cy3-labeled α-Syn was monomeric by performing photobleaching experiments. The results shown in Movie S2 demonstrated that immobilized labeled α-Syn photobleaches rapidly, as can be seen in the sample trajectory in Fig. S2 *C*. Statistical analysis (Fig. S2 *D*) demonstrates that 95% of cases were one-step bleaching events. Two-step processes were observed in 5% of cases and were assigned to dimer bleaching. Fifth, we need to take into consideration the ability of α-Syn to self-assemble into aggregates. The monomeric size of α-Syn was verified by AFM imaging (Fig. S4; see also Shlyakhtenko et al. (39)). This finding was in line with the low yield of two-step photobleaching experiments mentioned above (Fig. S2 *D*). A potential contribution to the observed fluorescence bursts from free-floating α-Syn is very small if any. Given the diffusion coefficient of α-Syn of $2 \times 10^{-6}$ $cm^2$ $s^{-1}$ (40), the characteristic time of translocation over the evanescent area (~100 nm) is ~0.1 ms, which is beyond the temporal resolution of the TIRF setup of the instrument (30 ms). The five factors just described were critical in developing the α-Syn immobilization procedure for reliable detection of the α-Syn dimerization process. The concentration of α-Syn for surface immobilization and the ratio between PEGs were optimized to reach the required surface coverage, as shown in Fig. S5.

## Visualization of α-Syn dimerization

Unlabeled WT α-Syn was tethered to the glass coverslip as described above, and the solution of fluorescently labeled WT α-Syn was placed on the top, so the binding process of labeled molecules to immobilized unlabeled WT α-Syn could be detected by continuous measuring of fluorescence by the TIRF system. This dimerization process can be seen in Movie S3 and Fig. S6, *A–C* (three frames from Movie S3). Bright spots on the image frames correspond to binding events, and the fluorescence duration defines the protein-complex lifetime. For example, fluorescence at spot 1 (Fig. S6, *A–C*, *circle 1*) is short, whereas spot 2 (*circle 2*) persists for a much longer time. These events

are quantitatively characterized by the time trajectories, and a selected set of such trajectories with different duration times is shown in Fig. 2. The peak in Fig. 2 *A* represents a complex formation event with a relatively short duration time, $\tau = 0.21$ s. Given the high stability of the fluorophore conjugated with $\alpha$-Syn, the abrupt drop in fluorescence intensity after 0.21 s was assigned to the dissociation of the complex rather than to photobleaching or photoblinking. Fig. 2, *B* and *C*, corresponded to longer lived complexes with lifetimes of 0.45 s and 1.29 s, respectively. Note the very long-lived event, with a lifetime of 6.63 s, in Fig. 2 *D*. It is important to note that all events had very similar fluorescence intensity, suggesting that complexes of the same stoichiometry are formed. The spots were predicted to be dimers formed by the immobilized $\alpha$-Syn and its fluorescent counterpart in solution. Trimerization would lead to a two-step dissociation pattern that was rarely observed in these experiments, since rather low concentrations of labeled $\alpha$-Syn were used. The process was reversible, as suggested by the fact that multiple dissociation and rebinding events were observed on the same trajectory for a selected target (Fig. S7). Fig. S7 *A* illustrates two consecutive binding-dissociation events at the same spot. The lifetimes of the dimers indicated in the graph are quite close. Fig. S7 *B* demonstrates three consecutive binding-dissociation events involving the same target. The initial event produces a dimer with a lifetime of 0.48 s, whereas the next events lead to the formation of dimers with shorter lifetimes.

Several hundreds of such events collected from different experiments were analyzed, and the data, assembled as histograms, are shown in Fig. 2 *E*. The majority of the events were grouped at a lifetime of ~0.2 s, although events as long as ~18 s could be found as well. The data were analyzed using the NSP approach, which does not require any assumptions about the type of data distribution (34,35). Graphs are shown in Fig. 2 *F*, and the entire data set is approximated by a double-exponential decay process, with distinct decay times of 197 ± 3 ms and 3334 ± 145 ms assigned to type 1 and type 2 dimers, respectively.

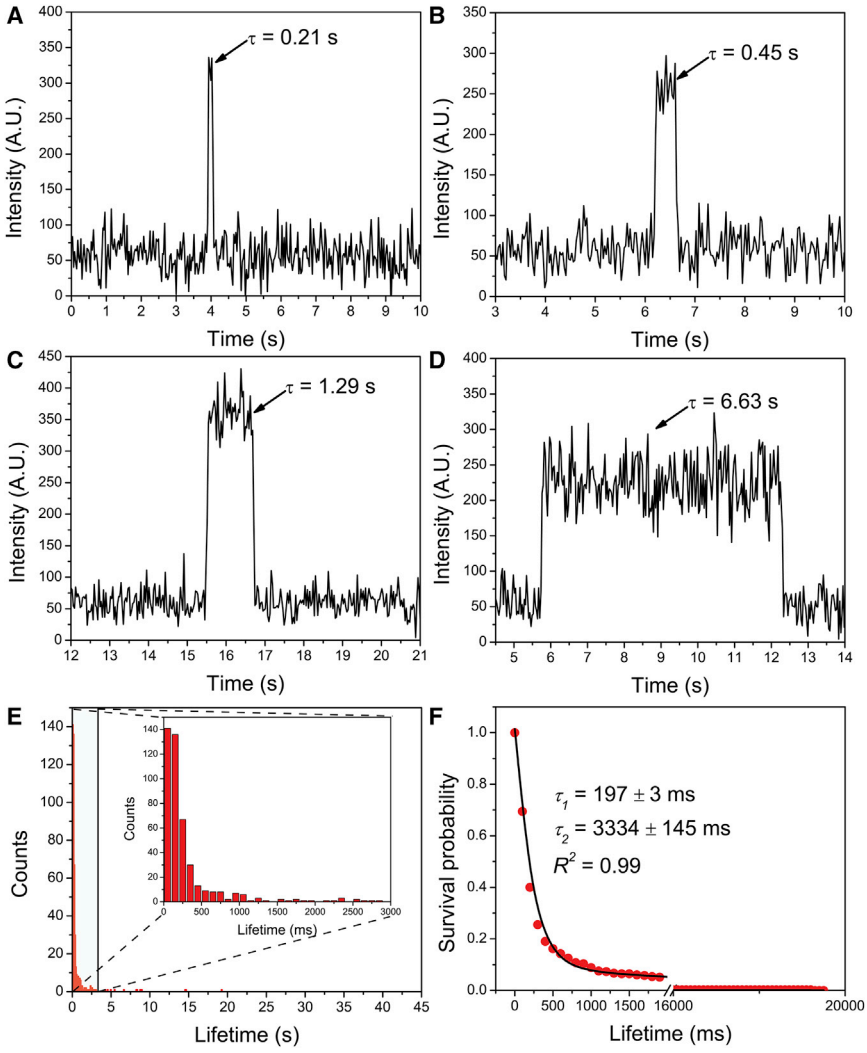


FIGURE 2 Typical fluorescence time traces of WT $\alpha$-Syn dimer with various lifetimes. Bursts of fluorescence (*arrows*) represent the formation of dimers by binding of a fluorophore-labeled $\alpha$-Syn to an immobilized $\alpha$-Syn on the surface with various lifetimes: 0.21 s (*A*), 0.45 s (*B*), 1.29 s (*C*), and 6.63 s (*D*). The concentrations of labeled $\alpha$-Syn in solution and unlabeled $\alpha$-Syn functionalized on the PEG-ylated surface are 1 nM and 25 pM, respectively. (*E*) Quantitative analysis of the fluorescence data. Histogram of lifetimes of WT $\alpha$-Syn dimer ($n = 462$). The majority of fluorescence bursts are shown in the inset of Fig. 2 *E*. (*F*) Normalized survival probability graph in which the red circles are normalized data points and the solid line is a fitting curve approximated by a two-exponential decay equation with lifetimes indicated in the graph. The errors are fitting errors. The *R*-squared value indicates the goodness of the fit. To see this figure in color, go online.

The population of type 1 dimers was the most abundant (90%), with only 10% of the detected dimers belonging to long-lived type 2 assemblies. In each individual experiment, two distinct lifetimes that differ by an order of magnitude were consistently observed. To further validate the type 2 dimer, the Kolmogorov-Smirnov test was used to test the difference between the two identified types of dimers. The results showed that the two types of dimer differ substantially from each other ($p < 0.01$) with respect to lifetime (Table S2).

## Effects of mutations on dimer stability

Similar analysis was performed with three $\alpha$-Syn mutants, A30P, E46K, and A53T, corresponding to familial mutations of Parkinson's disease. The experimental setup was similar to that for WT $\alpha$-Syn, described above. Each $\alpha$-Syn mutant was tethered to the coverslips, and the solution of the same fluorescently labeled $\alpha$-Syn mutant was placed on top of the coverslip to allow free $\alpha$-Syn molecules to interact with the immobilized counterpart. Complex formation was detected for these proteins as well (see Movies S4, S5, and S6). Time traces of representative dimer formation and dissociation events for A30P, E46K, and A53T $\alpha$-Syn mutants are shown in Figs. S8, S9, and S10, respectively. Similar to the results obtained with WT $\alpha$-Syn dimers, the lifetimes of mutant dimers varied in the range between several hundreds of milliseconds and several seconds. Histograms of dimer lifetimes for all mutants assembled over several hundred events are shown in Fig. 3, *A*, *C*, and *E*. The majority of lifetimes clustered at 0–0.5 s accompanied by spread-out events with lifetimes as long as several dozens of seconds. Compared with the WT $\alpha$-Syn data, which showed the majority of lifetimes clustered around 100 and 200 ms (Fig. 2 *E*), the lifetimes of mutants were shifted to larger values, indicating their higher dimer stability relative to the WT. Note the strong maximum of ~400 ms for the A30P mutant (Fig. 3 *A*). The NSP approach was applied to these data sets, and the resulting data for all mutants are shown in Fig. 3, *B*, *D*, and *F*. The

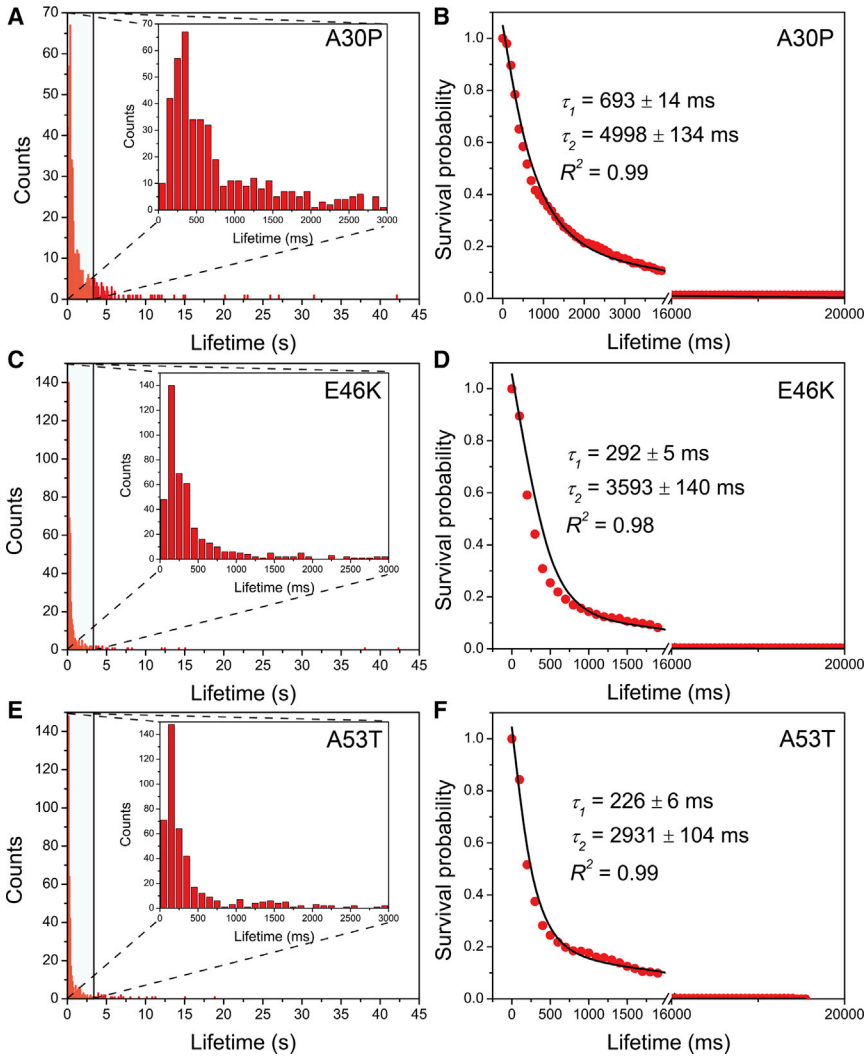


FIGURE 3 Quantitative analysis of the experiments with $\alpha$-Syn mutants A30P (*A* and *B*, $n = 505$), E46K (*C* and *D*, $n = 460$), and A53T (*E* and *F*, $n = 453$). The concentrations of labeled $\alpha$-Syn in solution and unlabeled $\alpha$-Syn functionalized on the PEG-ylated surface are 1 nM and 25 pM, respectively. (*Insets in A*, *C*, and *E*) Zooms of the graphs, showing the majority of the fluorescence bursts spanning 0–3 s. For each mutant dimer, the corresponding normalized survival probability is plotted against the lifetime and fitted with a two-exponential decay equation (*B*, *D*, and *F*). Red circles are normalized data points, solid lines are fitting curves, and lifetimes are shown in the graphs. The errors are fitting errors. *R*-squared values indicate the goodness of the fit. To see this figure in color, go online.

double-exponential decay was a good approximation for all data sets that led to lifetimes of type 1 dimers of A30P, E46K, and A53T of 693 ± 14 ms (Fig. 3 *B*), 292 ± 5 ms (Fig. 3 *D*), and 226 ± 6 ms (Fig. 3 *F*), respectively, averaged over three independent experiments. Altogether, the stability of type 1 dimers is arranged in the order A30P > E46K > A53T > WT. The lifetimes of type 2 dimers of A30P, E46K, and A53T were 4998 ± 134 ms, 3593 ± 140 ms, and 2931 ± 104 ms, respectively, so the stability of type 2 dimers (long-lived) decreases in the order A30P > E46K ≈ WT > A53T.

The distributions of type 1 and type 2 dimer populations are summarized in Fig. 4. Compared to WT dimers, E46K dimers had similar distribution (88% were type 1 dimer). A30P dimers had the smallest portion of type 1 dimers (78%) and possessed the longest lifetime of type 1 dimers among all the variants. The fraction of type 1 dimer for A53T (81%) was close to that of A30P but smaller than that of WT.

## DISCUSSION

### Conformational dynamics of α-Syn dimers

The proposed single-molecule fluorescence approach enabled us to quantitatively characterize interactions between α-Syn molecules. Using this approach, we demonstrated that the protein can form dimers with lifetimes in the range of a second that correspond to a barrier height as large as ~28 $k_BT$ (Table S3). Recently, the AFM force spectroscopy approach was applied to characterize α-Syn dimers (11,19,22), and the value of the dimer lifetime was also on a timescale in the range of seconds. However, AFM force spectroscopy probes dimer stability along the direction of the applied force. The correlation between the data obtained by two different techniques suggests that the dimer dissociation along the pulling direction has a similar barrier height. However, the fluorescence approach allowed us to identify dimers with substantially longer lifetimes of several seconds, termed type 2 dimers. Such stable α-Syn dimers were also identified in the AFM force spectroscopy experiments, but only at pH 2.7, whereas the fluorescence experiments used here were performed at neutral pH. The yield of rupture events of force measurements at neutral pH was very low, but measurements at pH 5.1 provided only one lifetime, $\tau = 0.23$ s (19). The fluorescence data show that the population of type 2 conformers of dimers is ~10%, so their detection with AFM force spectroscopy is problematic. Therefore, we infer that primarily type 1 conformers are detected in the AFM force spectroscopy experiments.

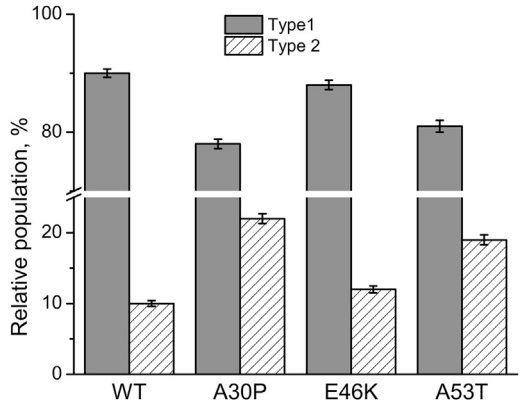


FIGURE 4 Relative populations of type 1 (short lifetime, *gray column*) and type 2 (long lifetime, *hatched column*) dimers of WT, A30P, E46K, and A53T dimers. The error bars are fitting errors.

The experimental approach described here consisted of an end-immobilization strategy involving the use of long flexible PEG tethers containing ~77 units of ethylene glycol that allowed the entire α-Syn molecule to adopt almost unrestricted conformations. In our force spectroscopy analysis of α-Syn (22,24), we showed that a C-terminal segment as long as ~30 residues was not involved in the interaction within the dimer, so tethering by the very end of the molecule does not interfere with dimer folding. Although the C-terminal domain of monomeric, unfolded α-Syn has been shown to interact with the central hydrophobic region via long-range interactions (41), the authors model the dimer interactions that occur with α-Syn molecules in solution under conditions where long-range interactions are relieved. Evidence suggests that the relief of these long-range interactions could promote dimerization and oligomerization (42). Moreover, any surface properties that may have influenced α-Syn dimerization in this study could be relevant to cellular oligomerization, based on evidence that membrane surfaces promote the self-assembly of α-Syn and other amyloidogenic proteins (43–45).

Although it has been widely assumed that the intracellular state of α-Syn is monomeric, the very recent studies of D. Selkoe et al. (46) suggest that α-Syn tetramers, rather than monomers, are the primary endogenous state of the protein, although others argue against this hypothesis (47,48). The long-lived dimers may form either potentially toxic oligomers (see below) or benign tetramers, and the distribution of these two outcomes is likely to vary among different α-Syn variants. We speculate that the difference between the two types of dimers observed here is in the stability of β-sheet structure, the major contributor to α-Syn fibril formation. This interpretation is supported by our recent computational analysis of dimers formed by amyloid β (14–23) dimers, which showed the formation of two stable amyloid β dimers with different stabilities, as defined by β-sheet size (29). We also speculate that long-lived dimer species may be more neurotoxic compared to short-lived species. This assumption is supported by a recent study (49) in which

the authors discovered two types of oligomer with distinct neurotoxicity.

### Role of mutations in α-Syn dimerization and aggregation

The comparative studies of WT α-Syn and all mutants (Figs. 2 and 3) demonstrate that mutations enhance the lifespan of type 1 dimer and that the lifetime values decay in the order A30P (693 ± 14 ms) > E46K (292 ± 5 ms) > A53T (226 ± 6 ms) > WT (197 ± 3 ms). These lifetimes correspond to energy barriers of 27.8 $k_BT$, 29.1 $k_BT$, 28.2 $k_BT$, and 28.0 $k_BT$ for WT, A30P, E46K, and A53T, respectively (Table S3). The longer lifetimes of type 1 dimers for the mutants compared with WT suggested that the single-point mutations promote dimerization along the type 1 pathway and eventually the entire aggregation process of α-Syn. The possibility that the dimeric species observed in this study may be species on the α-Syn self-assembly pathway leading to higher-order oligomers is suggested by the findings that 1) dimerization is a key step in α-Syn self-assembly (50–52); 2) familial α-Syn variants have been shown to have a high propensity to form oligomers (7); and 3) the data presented here suggest that familial mutations stabilize dimeric forms of α-Syn. Of the three mutations, A30P exerts the strongest effect on dimerization, causing a 3.5-fold increase in the lifetime of type 1 dimer over the lifetime for the WT. Only the A30P mutation increases the lifetime of long-lived type 2 dimers. However, all three mutations lead to an increase in the population of type 2 α-Syn dimer, although the effect depends on the mutation type. All but the A30P mutation accelerate α-Syn fibrillization kinetics (53,54), whereas A30P induces an increase in the rate of oligomerization (protofibril formation) (55,56). This particular mutant is different from the others, as well as from WT α-Syn, based on its very long lifetimes for both types of dimer and its relatively high population of type 2 dimers, which was more than twofold higher than that of WT α-Syn type 2 dimers. It has been shown recently that two structurally different α-Syn oligomers coexist for all four dimer species, A30P, E46K, A53T, and WT (57). One type of oligomer was reported to result in fibrillization, whereas the other was responsible for oligomerization. The A30P mutation only promotes oligomerization and retards fibrillization. Therefore, we speculate that oligomerization propensity depends on the ability to form long-lived dimers, and the high ratio between type 2 and type 1 A30P dimers promotes the oligomerization pathway. Additional dimer stabilization can be provided by oxidation (58,59) and/or nitration (60) processes that could promote protein aggregation in vivo.

Our finding that α-Syn forms dimers with different lifetimes yields insights into the potential mechanisms of α-Syn self-assembly. One possibility is that different types of α-Syn dimers form different types of assemblies, consistent with structural heterogeneity of oligomeric and fibrillar forms of α-Syn (8,15,49). Alternatively, some dimers could be precursors of potentially toxic α-Syn oligomers, whereas others are not (e.g., they could be precursors of benign tetramers). Additional evidence from future studies will be needed to determine which dimers lead to the formation of potentially toxic α-Syn oligomers and thus should be considered therapeutic targets. The data presented here support the interpretation from our earlier studies (24) that multiple contacts enhance the stability of dimeric, mutant α-Syn. In turn, this enhanced dimer stability increases the probability that dimeric α-Syn will proceed down the α-Syn self-assembly pathway toward oligomers instead of undergoing dissociation followed by rapid monomer remodeling (40,61).

## CONCLUSIONS

In summary, the single-molecule imaging approach developed here enabled us to measure the lifetimes of α-Syn dimers that appeared to be on a timescale in the range of seconds. Two classes of dimer with markedly different lifetimes were discovered. α-Syn mutations involved in the development of familial PD increase dimer stability, suggesting that the disease onset is defined by dimer formation, which is the very first aggregation event. Consistent with these findings, a previous study revealed that dimer formation was accelerated for the pathogenic A30P and A53T α-Syn mutants (50). The authors hypothesized that the effect was due to the greater propensity of mutants to self-interact, and our findings support this hypothesis. It is important to note that dimer formation was detected in solutions of nanomolar levels of α-Syn, suggesting that aggregation can occur at protein concentrations several orders of magnitude lower than those typically used in amyloid aggregation studies in solution in vitro. Although these low-concentration aggregation conditions were achieved in the protein-tethered setup, in which α-Syn was immobilized on the surface and dimers were formed by interaction of the immobilized protein with a freely diffusing α-Syn, the recent studies of Rabe et al. (62) showed that tethering of the protein is not required and that aggregation of α-Syn from a nanomolar-range solution can occur at the surface-liquid interface. Moreover, aggregation on the surface occurs more rapidly than in solution, regardless of the very high protein concentration in solution, which is several orders of magnitude higher than the concentrations used in the on-surface aggregation studies. Surfaces of various types are ubiquitous for intracellular and extracellular compartments, so it is highly important to understand the acceleration effect of surfaces in the protein self-assembly process. The approach described in this article showed that the very first self-assembly step, with the participation of the tethered protein, occurs at a subnanomolar protein concentration in solution and leads to the formation of stable dimers

presumably in their misfolded state. The use of long-lived fluorophores (30,63) makes it possible to extend these studies to the quantitative analysis of later self-assembly stages such as trimer and tetramer, and work in this regard is in progress. Note as well that the described tethered approach is general and can be applied to any protein that undergoes misfolding and self-assembly.

## SUPPORTING MATERIAL

Supporting Materials and Methods, Supporting Results, 11 figures, three tables, and six movies are available at http://www.biophysj.org/biophysj/supplemental/S0006-3495(15)00243-X.

## AUTHOR CONTRIBUTIONS

Z.L., A.V.K. and Y.L.L. designed the experiments. D.Y. and J.C.R. produced $\alpha$-Syn proteins. S.C.B. provided fluorophores. Z.L. and Y.Z. performed the experiments and analyzed the data. Z.L., A.V.K., Y.Z. and Y.L.L. discussed the results and wrote the manuscript. All authors reviewed the manuscript.

## ACKNOWLEDGMENTS

This work was supported by grants GM096039 (National Institutes of Health) and EPS-1004094 (National Science Foundation) to Y.L.L., grant GM098859 to S.C.B., and a grant from the Branfman Family Foundation to J.C.R.

## REFERENCES

1. Dawson, T. M., and V. L. Dawson. 2003. Molecular pathways of neurodegeneration in Parkinson's disease. *Science.* 302:819–822.
2. Goedert, M., M. G. Spillantini, …, H. Braak. 2013. 100 years of Lewy pathology. *Nat. Rev. Neurol*. 9:13–24.
3. Jarrett, J. T., and P. T. Lansbury, Jr. 1993. Seeding "one-dimensional crystallization" of amyloid: a pathogenic mechanism in Alzheimer's disease and scrapie? *Cell.* 73:1055–1058.
4. Lashuel, H. A., C. R. Overk, …, E. Masliah. 2013. The many faces of $\alpha$-synuclein: from structure and toxicity to therapeutic target. *Nat. Rev. Neurosci.* 14:38–48.
5. Deleersnijder, A., M. Gerard, …, V. Baekelandt. 2013. The remarkable conformational plasticity of $\alpha$-synuclein: blessing or curse? *Trends Mol. Med.* 19:368–377.
6. Bendor, J. T., T. P. Logan, and R. H. Edwards. 2013. The function of $\alpha$-synuclein. *Neuron.* 79:1044–1066.
7. Breydo, L., J. W. Wu, and V. N. Uversky. 2012. A-synuclein misfolding and Parkinson's disease. *Biochim. Biophys. Acta.* 1822:261–285.
8. Heise, H., W. Hoyer, …, M. Baldus. 2005. Molecular-level secondary structure, polymorphism, and dynamics of full-length $\alpha$-synuclein fibrils studied by solid-state NMR. *Proc. Natl. Acad. Sci. USA.* 102:15871–15876.
9. Vilar, M., H. T. Chou, …, R. Riek. 2008. The fold of $\alpha$-synuclein fibrils. *Proc. Natl. Acad. Sci. USA.* 105:8637–8642.
10. Brucale, M., B. Schuler, and B. Samori. 2014. Single-molecule studies of intrinsically disordered proteins. *Chem. Rev.* 114:3281–3317.
11. Lyubchenko, Y. L., B. H. Kim, …, J. Yu. 2010. Nanoimaging for protein misfolding diseases. *Wiley Interdiscip. Rev. Nanomed. Nanobiotechnol.* 2:526–543.
12. Sandal, M., F. Valle, …, B. Samorì. 2008. Conformational equilibria in monomeric $\alpha$-synuclein at the single-molecule level. *PLoS Biol.* 6:e6.
13. Brucale, M., M. Sandal, …, B. Samorì. 2009. Pathogenic mutations shift the equilibria of $\alpha$-synuclein single molecules towards structured conformers. *ChemBioChem.* 10:176–183.
14. Hervás, R., J. Oroz, …, M. Carrión-Vázquez. 2012. Common features at the start of the neurodegeneration cascade. *PLoS Biol.* 10:e1001335.
15. Neupane, K., A. Solanki, …, M. T. Woodside. 2014. Diverse metastable structures formed by small oligomers of $\alpha$-synuclein probed by force spectroscopy. *PLoS ONE.* 9:e86495.
16. Trexler, A. J., and E. Rhoades. 2010. Single molecule characterization of $\alpha$-synuclein in aggregation-prone states. *Biophys. J.* 99:3048–3055.
17. Ferreon, A. C., Y. Gambin, …, A. A. Deniz. 2009. Interplay of $\alpha$-synuclein binding and conformational switching probed by single-molecule fluorescence. *Proc. Natl. Acad. Sci. USA.* 106:5645–5650.
18. Straub, J. E., and D. Thirumalai. 2011. Toward a molecular theory of early and late events in monomer to amyloid fibril formation. *Annu. Rev. Phys. Chem.* 62:437–463.
19. Yu, J., S. Malkova, and Y. L. Lyubchenko. 2008. $\alpha$-Synuclein misfolding: single molecule AFM force spectroscopy study. *J. Mol. Biol.* 384:992–1001.
20. Kim, B. H., N. Y. Palermo, …, Y. L. Lyubchenko. 2011. Single-molecule atomic force microscopy force spectroscopy study of A$\beta$-40 interactions. *Biochemistry.* 50:5154–5162.
21. Yu, J., J. Warnke, and Y. L. Lyubchenko. 2011. Nanoprobing of $\alpha$-synuclein misfolding and aggregation with atomic force microscopy. *Nanomedicine* (*Lond.*). 7:146–152.
22. Krasnoslobodtsev, A. V., J. Peng, …, Y. L. Lyubchenko. 2012. Effect of spermidine on misfolding and interactions of $\alpha$-synuclein. *PLoS ONE.* 7:e38099.
23. Portillo, A. M., A. V. Krasnoslobodtsev, and Y. L. Lyubchenko. 2012. Effect of electrostatics on aggregation of prion protein Sup35 peptide. *J. Phys. Condens. Matter.* 24:164205.
24. Krasnoslobodtsev, A. V., I. L. Volkov, …, Y. L. Lyubchenko. 2013. $\alpha$-Synuclein misfolding assessed with single molecule AFM force spectroscopy: effect of pathogenic mutations. *Biochemistry.* 52:7377–7386.
25. Lv, Z., M. M. Condron, …, Y. L. Lyubchenko. 2013. Nanoprobing of the effect of $Cu^{2+}$ cations on misfolding, interaction and aggregation of amyloid $\beta$ peptide. *J. Neuroimmune Pharmacol.* 8:262–273.
26. Lv, Z., R. Roychaudhuri, …, Y. L. Lyubchenko. 2013. Mechanism of amyloid $\beta$-protein dimerization determined using single-molecule AFM force spectroscopy. *Sci. Rep*. 3:2880.
27. Shlyakhtenko, L. S., A. A. Gall, and Y. L. Lyubchenko. 2013. Mica functionalization for imaging of DNA and protein-DNA complexes with atomic force microscopy. *Methods Mol. Biol.* 931:295–312.
28. Kim, B. H., and Y. L. Lyubchenko. 2014. Nanoprobing of misfolding and interactions of amyloid $\beta$ 42 protein. *Nanomedicine* (*Lond.*). 10:871–878.
29. Lovas, S., Y. Zhang, …, Y. L. Lyubchenko. 2013. Molecular mechanism of misfolding and aggregation of A$\beta$(13–23). *J. Phys. Chem. B.* 117:6175–6186.
30. Zheng, Q., M. F. Juette, …, S. C. Blanchard. 2014. Ultra-stable organic fluorophores for single-molecule research. *Chem. Soc. Rev.* 43:1044–1056.
31. Lee, H. W., T. Kyung, …, T. Y. Yoon. 2013. Real-time single-molecule co-immunoprecipitation analyses reveal cancer-specific Ras signalling dynamics. *Nat. Commun.* 4:1505.
32. Lamboy, J. A., H. Kim, …, E. A. Komives. 2011. Visualization of the nanospring dynamics of the I$\kappa$B$\alpha$ ankyrin repeat domain in real time. *Proc. Natl. Acad. Sci. USA.* 108:10178–10183.
33. Roy, R., S. Hohng, and T. Ha. 2008. A practical guide to single-molecule FRET. *Nat. Methods.* 5:507–516.

34. Bayas, M. V., A. Leung, …, D. Leckband. 2006. Lifetime measurements reveal kinetic differences between homophilic cadherin bonds. *Biophys. J.* 90:1385–1395.

35. Karymov, M. A., A. V. Krasnoslobodtsev, and Y. L. Lyubchenko. 2007. Dynamics of synaptic SfiI-DNA complex: single-molecule fluorescence analysis. *Biophys. J.* 92:3241–3250.

36. Tinoco, Jr., I., and C. Bustamante. 2002. The effect of force on thermodynamics and kinetics of single molecule reactions. *Biophys. Chem.* 101-102:513–533.

37. Powell, L. R., K. D. Dukes, and R. K. Lammi. 2012. Probing the efficacy of peptide-based inhibitors against acid- and zinc-promoted oligomerization of amyloid-$\beta$ peptide via single-oligomer spectroscopy. *Biophys. Chem.* 160:12–19.

38. Zheng, Q., S. Jockusch, …, S. C. Blanchard. 2012. On the mechanisms of cyanine fluorophore photostabilization. *J. Phys. Chem. Lett*. 3:2200–2203.

39. Shlyakhtenko, L. S., J. Gilmore, …, Y. L. Lyubchenko. 2009. Molecular mechanism underlying RAG1/RAG2 synaptic complex formation. *J. Biol. Chem.* 284:20956–20965.

40. Ahmad, B., Y. Chen, and L. J. Lapidus. 2012. Aggregation of $\alpha$-synuclein is kinetically controlled by intramolecular diffusion. *Proc. Natl. Acad. Sci. USA*. 109:2336–2341.

41. Dedmon, M. M., K. Lindorff-Larsen, …, C. M. Dobson. 2005. Mapping long-range interactions in $\alpha$-synuclein using spin-label NMR and ensemble molecular dynamics simulations. *J. Am. Chem. Soc.* 127:476–477.

42. Bertoncini, C. W., Y. S. Jung, …, M. Zweckstetter. 2005. Release of long-range tertiary interactions potentiates aggregation of natively unstructured $\alpha$-synuclein. *Proc. Natl. Acad. Sci. USA*. 102:1430–1435.

43. Cao, P., A. Abedini, and D. P. Raleigh. 2013. Aggregation of islet amyloid polypeptide: from physical chemistry to cell biology. *Curr. Opin. Struct. Biol.* 23:82–89.

44. Pandey, A. P., F. Haque, …, J. S. Hovis. 2011. $\alpha$-Synuclein-induced tubule formation in lipid bilayers. *J. Phys. Chem. B.* 115:5886–5893.

45. Haque, F., A. P. Pandey, …, J. S. Hovis. 2010. Adsorption of $\alpha$-synuclein on lipid bilayers: modulating the structure and stability of protein assemblies. *J. Phys. Chem. B.* 114:4070–4081.

46. Selkoe, D., U. Dettmer, …, T. Bartels. 2014. Defining the native state of $\alpha$-synuclein. *Neurodegener. Dis.* 13:114–117.

47. Fauvet, B., M. K. Mbefo, …, H. A. Lashuel. 2012. $\alpha$-Synuclein in central nervous system and from erythrocytes, mammalian cells, and *Escherichia coli* exists predominantly as disordered monomer. *J. Biol. Chem.* 287:15345–15364.

48. Burre, J., S. Vivona, …, T. C. Sudhof. 2013. Properties of native brain $\alpha$-synuclein. *Nature*. 498:E4–E6, discussion E6–E7.

49. Cremades, N., S. I. Cohen, …, D. Klenerman. 2012. Direct observation of the interconversion of normal and toxic forms of $\alpha$-synuclein. *Cell.* 149:1048–1059.

50. Krishnan, S., E. Y. Chi, …, J. F. Carpenter. 2003. Oxidative dimer formation is the critical rate-limiting step for Parkinson's disease $\alpha$-synuclein fibrillogenesis. *Biochemistry.* 42:829–837.

51. Pivato, M., G. De Franceschi, …, L. Bubacco. 2012. Covalent $\alpha$-synuclein dimers: chemico-physical and aggregation properties. *PLoS ONE.* 7:e50027.

52. Roostaee, A., S. Beaudoin, …, X. Roucou. 2013. Aggregation and neurotoxicity of recombinant $\alpha$-synuclein aggregates initiated by dimerization. *Mol. Neurodegener.* 8:5.

53. Conway, K. A., J. D. Harper, and P. T. Lansbury. 1998. Accelerated in vitro fibril formation by a mutant $\alpha$-synuclein linked to early-onset Parkinson disease. *Nat. Med.* 4:1318–1320.

54. Greenbaum, E. A., C. L. Graves, …, B. I. Giasson. 2005. The E46K mutation in $\alpha$-synuclein increases amyloid fibril formation. *J. Biol. Chem.* 280:7800–7807.

55. Conway, K. A., S. J. Lee, …, P. T. Lansbury, Jr. 2000. Acceleration of oligomerization, not fibrillization, is a shared property of both $\alpha$-synuclein mutations linked to early-onset Parkinson's disease: implications for pathogenesis and therapy. *Proc. Natl. Acad. Sci. USA*. 97:571–576.

56. Li, J., V. N. Uversky, and A. L. Fink. 2001. Effect of familial Parkinson's disease point mutations A30P and A53T on the structural properties, aggregation, and fibrillation of human $\alpha$-synuclein. *Biochemistry.* 40:11604–11613.

57. Paslawski, W., S. Mysling, …, D. E. Otzen. 2014. Co-existence of two different $\alpha$-synuclein oligomers with different core structures determined by hydrogen/deuterium exchange mass spectrometry. *Angew. Chem. Int. Ed. Engl.* 53:7560–7563.

58. Liu, F., J. Hindupur, …, J. C. Rochet. 2008. Methionine sulfoxide reductase A protects dopaminergic cells from Parkinson's disease-related insults. *Free Radic. Biol. Med.* 45:242–255.

59. Swomley, A. M., S. Förster, …, D. A. Butterfield. 2014. A$\beta$, oxidative stress in Alzheimer disease: evidence based on proteomics studies. *Biochim. Biophys. Acta.* 1842:1248–1257.

60. Stone, D. K., T. Kiyota, …, H. E. Gendelman. 2012. A model of nitric oxide induced $\alpha$-synuclein misfolding in Parkinson's disease. *Neurosci. Lett.* 523:167–173.

61. Lapidus, L. J. 2013. Understanding protein aggregation from the view of monomer dynamics. *Mol. Biosyst.* 9:29–35.

62. Rabe, M., A. Soragni, …, S. Seeger. 2013. On-surface aggregation of $\alpha$-synuclein at nanomolar concentrations results in two distinct growth mechanisms. *ACS Chem. Neurosci.* 4:408–417.

63. Altman, R. B., D. S. Terry, …, S. C. Blanchard. 2012. Cyanine fluorophore derivatives with enhanced photostability. *Nat. Methods.* 9:68–71.

# Supporting material

**Direct Detection of α-Synuclein Dimerization Dynamics: Single-molecule Fluorescence Analysis**

Zhengjian Lv[#], Alexey V. Krasnoslobodtsev[#], Yuliang Zhang[#], Daniel Ysselstein[‡], Jean-Christophe Rochet[‡], Scott Blanchard[¶] and Yuri L. Lyubchenko[#]*.

## Supporting materials and methods

### α-Synuclein Proteins

Wild-type A140C α-synuclein in which the C-terminal alanine was replaced with a cysteine and the double mutants A30P-A140C, A53T-A140C and E46K-A140C were prepared as described in(1, 2). cDNAs encoding double cysteinyl α-Syn variant (V3C-A140C) was amplified by PCR and subcloned as Nde I – Hind III fragments into the vector pT7-7. The sequence of the a-Syn-encoding insert in each construct was verified using an Applied Biosystems (ABI 3730 XL) DNA sequencer. The double cysteinyl α-Syn variant was expressed in the E. coli strain BL21 (DE3) and purified as described(1, 2). Each α-Syn variant was further purified by reverse phase high performance liquid chromatography and analyzed by matrix assisted laser desorption ionization (MALDI) mass spectrometry. The mass-to-charge (m/z) values obtained from the MALDI analysis corresponded to the predicted values for full-length α-Syn.

### Labeling of α-Syn with fluorophore

α-Syn solutions were freshly prepared by dissolving 0.4 to 0.8 mg of the lyophilized powder in 200 μL pH 11 water, with the addition of 1 μL of 1 M dithiothreitol (DTT) to break disulfide bonds, followed by the addition of 300 μL of pH 7.0 PBS buffer. The obtained solution was filtered through an Amicon filter with a molecular weight cutoff of 10 kDa at 14000 rpm for 15 min to remove free DTT. The filtration was repeated 3 times. The concentration of α-Syn in the solutions was determined by spectrophotometry (Nanodrop® ND-1000, DE) using the molar extension coefficients 1280 $cm^{-1} \cdot m^{-1}$ and 120 $cm^{-1} \cdot m^{-1}$ for tyrosine and cysteine at 280 nm, respectively. Aliquots were stored at – 20 $^{o}$C.

Single cysteinyl α-Syn (with a cysteine residue at the C terminus) and double cysteinyl α-Syn (with two cysteine residues at both the N and C terminus) were labeled with ultra-stable Cy3 and regular Cy3, respectively, both containing a maleimide functional group. When labeling single cysteinyl α-Syn, excess ultra-stable Cy3 was added (the ratio between ultra-stable Cy3 and α-Syn was 10:1). When labeling double cysteinyl α-Syn, the ratio between regular Cy3 and α-Syn was 1:1. α-Syn was mixed with fluorophores and subjected to intermittent gentle vortexing. The reaction was kept in the dark at room temperature. After 2 h, the mixture was added to ~300 μL of PBS buffer and filtered through an Amicon filter (molecular weight cutoff = 10 kDa) at 14000 rpm for 15 min to remove free fluorophores. The filtration was repeated 3 times. The filtrate was discarded and the retentate was collected. The concentration of each fluorophore-labeled α-Syn was determined by spectrophotometry, using equation 1. The absorbance of the fluorophore at 280 nm was approximately 8% of that at 552 nm, and this value was subtracted when measuring protein concentration at 280 nm using the following equation:

$$C_{a-syn} = \frac{[A_{280} - (0.08 \times A_{552})]}{\varepsilon_{a-syn}} \qquad (1)$$

The labeling efficiency was calculated using the following equation:

$$labeling\ efficiency\ (\%) = \frac{\left(\frac{\varepsilon_{a-syn}}{\varepsilon_{fluorophore}} \times A_{552}\right)}{[A_{280} - (0.08 \times A_{552})]} \times 100 \qquad (2)$$

The labeling efficiency for single cysteinyl α-Syn and double cysteinyl α-Syn was 40-50% and 22-25%, respectively. Stock solutions and aliquots were stored at – 20°C under inert (argon) atmosphere.

## Single-molecule photobleaching

Coverslips were first functionalized with 167 μM APS, followed by functionalization with mixed PEG (mPEG-SVA: MAL-PEG-SVA = 100:1). The double cysteinyl α-Syn with commercially available Cy 3 labeled at one end was immobilized onto the PEG-lated surface through the other end. The covalent immobilization of Cy 3 onto the PEG-lated surface ensured that fluorophores were under constant excitation and emission. Single-molecule photobleaching experiments were conducted on an Olympus IX71 instrument, with the same setup as regular experiments. The

video was recorded with ~ 30 s duration. Fluorophores from commercial sources usually bleach within this time window.

## AFM imaging

APS-mica was used in AFM experiments. Mica strips (5.0×1.5 cm) were freshly cleaved and functionalized by immersion into aqueous 167 μM APS solution for 30 min. APS-mica was then thoroughly rinsed with DI water, dried with argon flow and stored in a vacuum chamber. The APS-mica strip was cut into ~0.75×0.75 cm pieces for the sample preparation. α-Syn samples were diluted from freshly prepared stock solution to 10 nM with pH 7.0 10 mM PBS buffer. 8 μL of diluted samples were deposited onto APS-mica surfaces for 2 min, followed by a thorough rinse with DI water. The specimens were dried with argon flow and kept in a vacuum chamber overnight. Next, the specimens were mounted onto metal discs with double-side tape.

AFM imaging was performed on a multimode 8 AFM (Bruker Nano, Santa Barbara, CA) equipped with PeakForce modules. Images were acquired in air using MSNL tips (Bruker Nano, Santa Barbara, CA) with a nominal spring constant of 0.5 N/m. AFM images were scanned with 512×512 pixels at rates of 4-6 Hz. AFM images were flattened by Nanoscope Analysis (Bruker Nano, Santa Barbara, CA). Volume analysis of fresh α-Syn samples was conducted using Femtoscan (Advanced Technologies Center, Moscow, Russia) software. “Enum features”, a functional tool provided by the software, was used to measure volumes of the protein on AFM images. The background was subtracted over the non-covered surface area. The volume values were obtained and then subjected to a Gaussian fit using Origin 6.0 software.

## Supplementary results

To test the photophysical properties of ultra-stable fluorophores, fluorophores were covalently immobilized to the cover slip via SVA-PEG-SVA (SVA-PEG-SVA: mPEG = 1:100), of which one NHS group was used to link to the APS on the substrate while the other one was used for fluorophore conjugation. The data showed the majority of ultra-stable fluorophores did not bleach and blink during the data acquisition time (Supplementary movie 1). An example of a time trajectory of dye intensity is shown in Fig. S1. Overall, the fluorophores did not photobleach or photoblink within the data acquisition time.

α-Syn that contains two cysteines at the N- and C-terminus was labeled with regular Cy3

at one end, whereas the other end was used for conjugation with a Mal-PEG-SVA-functionalized cover slip. Bright spots are sparsely observed in Figure S2A, suggesting the homogeneity of surface coverage. There were no such spots on an mPEG-SVA functionalized surface, suggesting that non-specific binding of α-Syn is very low (Fig. S2B). To see if any fluorophore-labeled single cysteinyl α-Syn molecule nonspecifically adsorbed onto the surface, 1 nM of Cy3-labeled single cysteinyl α-Syn was added on a mixed PEG surface and imaged with TIRF (Fig. S3A). The number of nonspecifically adsorbed particles was then counted. The ratio of nonspecific adsorption events to specific binding events was substantially lower than 10%(3), a threshold number used for evaluating the fidelity of single-molecule detection. To examine if mPEG-SVA successfully passivated the substrate, 1 nM of fluorophore-labeled single cysteinyl α-Syn was directly deposited on an untreated glass slide and imaged with TIRF (Fig. S3B). The adsorbed particles were then spotted. A large number of fluorophores are observed because of strong nonspecific adsorption. The insets in Fig. S3A and Fig. S3B show schematics of individual experimental designs. The backgrounds of Fig. S3A and Fig. S3B are intentionally adjusted at the same level for better comparison. The latter two controls showed mPEG-SVA was suitable and capable of eliminating nonspecific adsorption. We next performed photobleaching experiments to ensure that immobilized α-Syn molecules were indeed single-molecules. A typical photobleaching trace is shown in Fig S2C. Over 95% of traces displayed single-step bleaching (Fig. S2D), suggesting that appropriate conditions for the single-molecule fluorescence experiments were identified. Only a few traces showed two-step bleaching, suggesting that colocalization of two α-Syn molecules within the excitation spot is a rare event. Third, we examined the self-assembling ability of α-Syn into aggregates. The protein stoichiometry in solution was inspected by AFM imaging (Fig. S4A). The protein appeared as small globular particles (blobs) of uniform size (Fig. S4B) corresponding to the monomeric size of the protein(4).

By optimizing the concentrations of α-Syn and the ratio between PEGs, well separated dimeric complexes of α-Syn molecules were acquired with sufficient yields at 1 nM of fluorophore-labeled α-Syn for injection, 25 pM fluorophore-free α-Syn for immobilization, and 1:100 of MAL-PEG-SVA: mPEG-SVA for surface passivation (Fig. S5). Two dimerization events from the same movie are shown in Fig. S6. Only the area of interest is shown. Spots of interest are highlighted and numbered 1 and 2. At frame A, there are fluorophores existing on

both spots, indicating the occurrence of dimerization events. At frame B, fluorophore 1 (spot 1) flies away after a short dwell, while fluorophore 2 (spot 2) stays for a longer time until frame C. Assemblies of typical fluorescence time traces of dimerization events of A30P, 4E6K and A53T are shown in Figs. S8, S9 and S10, respectively.

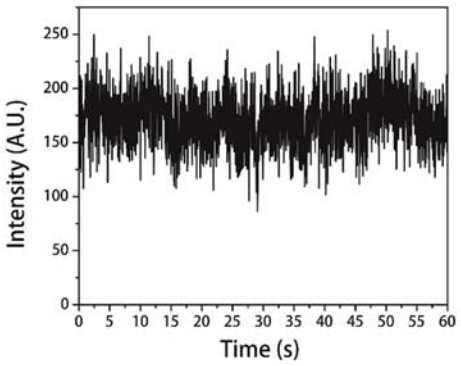


Figure S1. A time trajectory of an ultra-stable fluorophore covalently linked to the substrate via SVA-PEG-SVA.

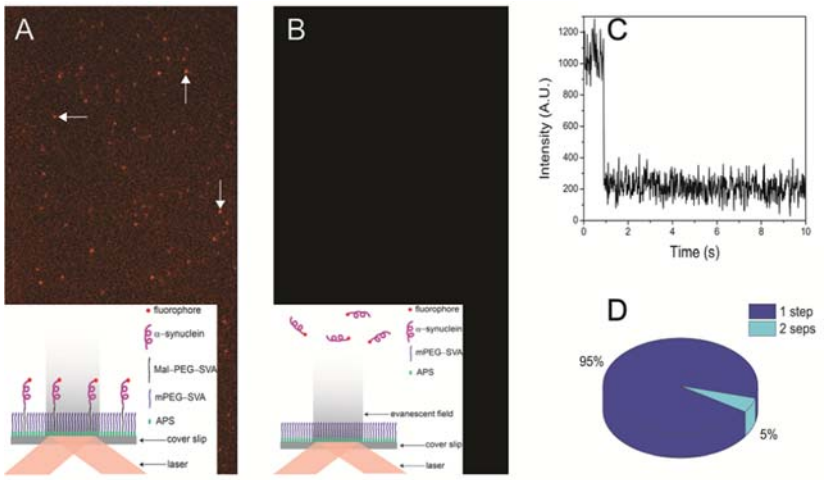


Figure S2. Selected frames of the fluorescence intensities for (A) immobilized Cy3 α-Syn and (B) control experiment involving the omission of Mal-PEG-SVA, thereby preventing covalent immobilization of Cys-α-Syn. Arrows in panel A point to selected typical dyes that continuously fluoresce until bleach. The insets in A and B show schematics for each experimental setup. (C) A single-molecule photobleaching trace shows typical one-step bleaching. (D) Pie histogram for the distribution of one-step and two-step bleaching events. The background levels in A and B were adjusted at the same values.

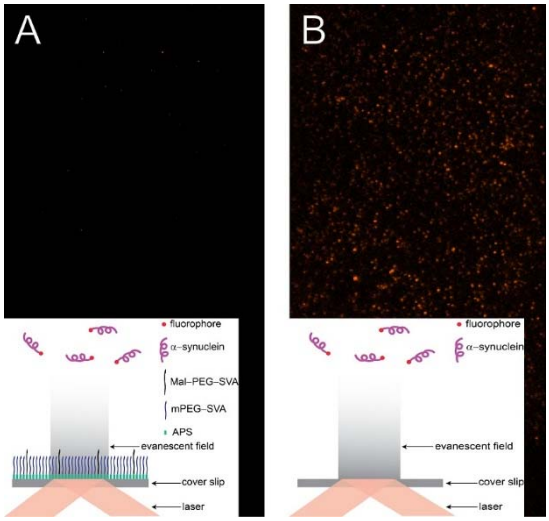


Figure S3. Comparison of 1 nM labeled α-Syn non-specific adsorption on various surfaces. (A) Non-specific adsorption on the mixed PEG-functionalized surface. (B) Adsorption of the same labeled α-Syn on a clean cover slip.

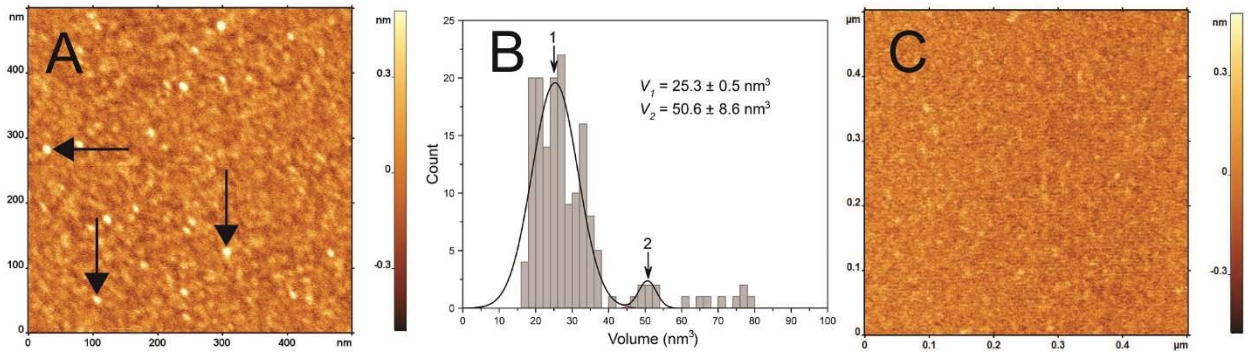


Figure S4. AFM analysis of the WT a-Syn sample. (A) AFM image (500 nm × 500 nm) in which arrows point to spherical features corresponding to α-Syn molecules. The Z scale has a maximum of 0.5 nm. (B) Histogram showing the distribution of volumes obtained from measurements of 165 α-Syn molecules. Two peaks corresponding to monomer (25.3 ± 0.5 nm$^3$) and dimer (50.6 ± 8.6 nm$^3$) are clearly shown. Two deconvolved individual fits are well overlaid with the sum that is shown as the black solid line. The ratio between monomer and dimer is estimated to be 94:6. (C) AFM image of a sample from a control experiment in which only buffer without the protein was imaged (500 nm × 500 nm).

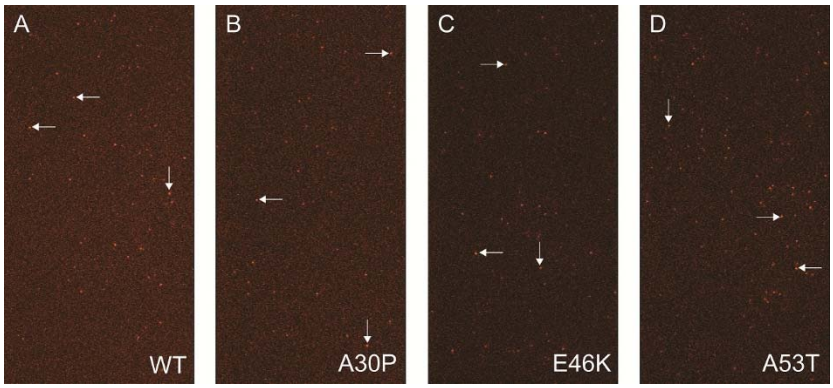


Figure S5. Snapshots of the dimerization events for WT (A), A30P (B), E46K (C) and A53T (D), respectively. Arrows indicate a few typical dimer formation events. The ratios between Mal-PEG-SVA and mPEG was 1:100.

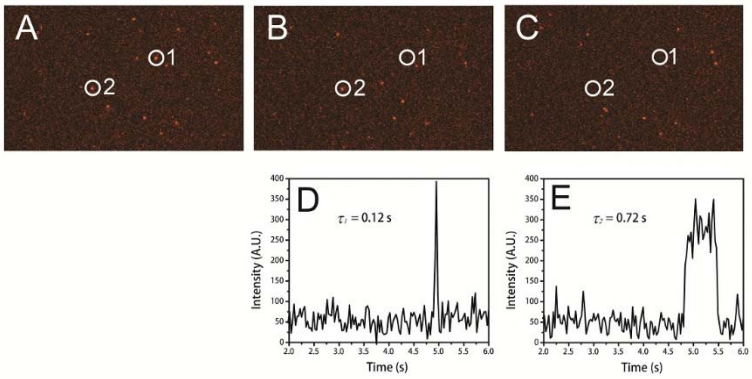


Figure S6. Three frames (A, B and C) taken from supplementary movie 1, which show two dimerization events with different lifetimes. The corresponding traces of spots 1 and 2 are shown in D and E, respectively.

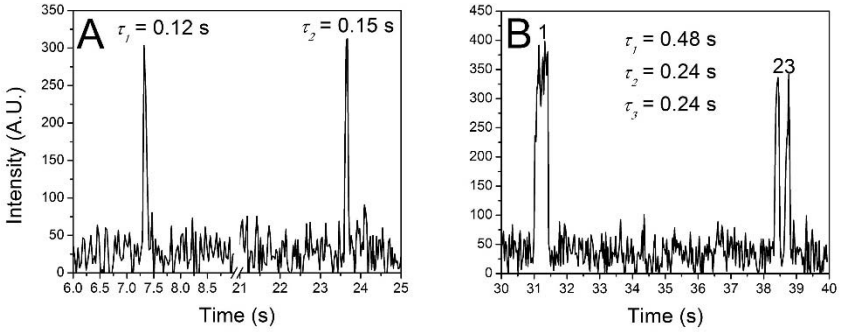


Figure S7. Multiple dissociation and rebinding events observed along the same time trajectory for WT α-Syn. (A) two dimerization events separated with a long time interval. (B) Three dimerization events observed in a time interval of less than 10 s. Event 3 appeared in less than 2 s after event 2. The lifetimes for each event are indicated.

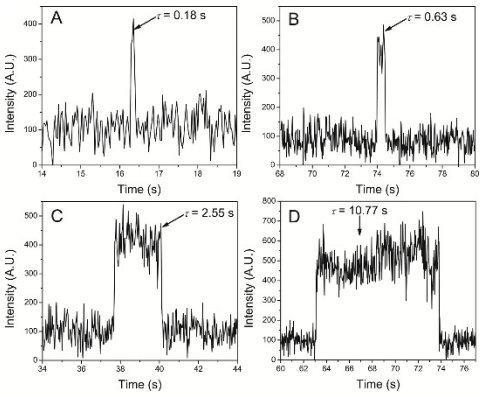


Figure S8. Typical fluorescence time traces of four events for A30P dimer. The lifetimes are indicated.

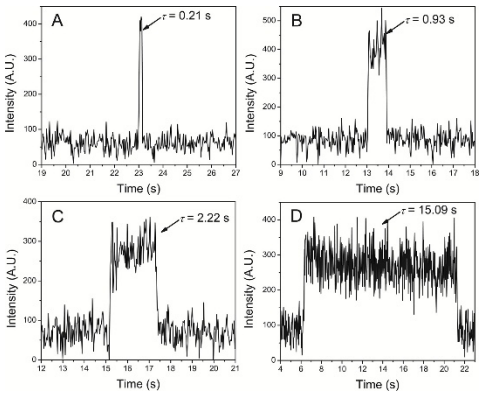


Figure S9. Typical fluorescence time traces of four events for E46K dimer. The lifetimes are indicated.

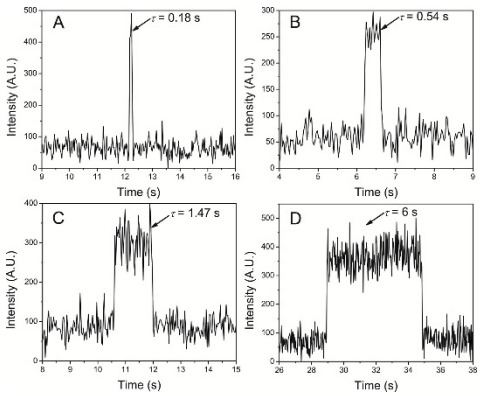


Figure S10. Typical fluorescence time traces of four events for A53T dimer. The lifetimes are indicated.

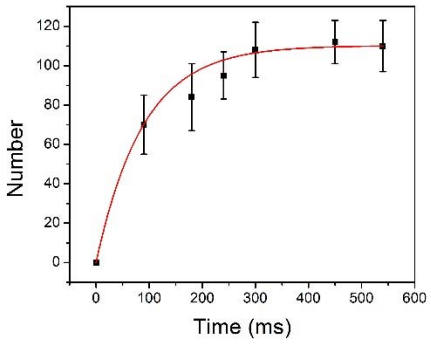


Figure S11. Time dependence of α–Syn dimerization events during the initial twenty frames. This graph shows that a plateau is reached at ~300 ms. Numbers are averaged over at least three consecutive frames. Error bars indicate ± SD.

## Supplementary tables

Table S1. Comparison of goodness-of-fitting ($R^2$) among single exponential (1-exp), double exponential (2-exp), and triple exponential (3-exp) decays for α-Syn proteins.

| | $R^2$ (1-exp) | Lifetime (ms) | $R^2$ (2-exp) | Lifetime (ms) | $R^2$ (3-exp) | Lifetime (ms) |
|---|---|---|---|---|---|---|
| WT | 0.96 | $\tau$ = 278 ± 9 | 0.99 | $\tau_1$ = 197 ± 3<br>$\tau_2$ = 3334 ± 145 | 0.99 | $\tau_1$ = 170 ± 6<br>$\tau_2$= 1.7 [a]<br>$\tau_3$ = 3262 ± 197 |
| A30P | 0.95 | $\tau$ = 1486 ± 30 | 0.99 | $\tau_1$ = 693 ± 14<br>$\tau_2$ = 4998 ± 134 | 0.99 | $\tau_1$ = 506 ± 20<br>$\tau_2$ = 2160 ± 137<br>$\tau_3$ = 11328 ± 881 |
| E46K | 0.93 | $\tau$ = 465 ± 11 | 0.98 | $\tau_1$ = 292 ± 5<br>$\tau_2$ = 3593 ± 140 | Fit does not converge [b] | NA |
| A53T | 0.88 | $\tau$ = 529 ± 25 | 0.99 | $\tau_1$ = 226 ± 6<br>$\tau_2$ = 2931 ± 104 | 0.99 | $\tau_1$ = 226 ± 5 [c]<br>$\tau_2$ = 2931 ± 122 [c] |

Note: [a] the obtained value of fitting parameters $A_2$ is negative; [b] failure to perform 3-exp fit; [c] 3-exp fit gives two but not three lifetimes.

Table S2. Lifetimes of four protein dimers from individual experiments

| **Sample** | **Experiment number** | $\tau_1$ (ms, ± fitting error) | $\tau_2$ (ms, ± fitting error) |
|---|---|---|---|
| WT | 1 | 159 ± 6 | 2675 ± 1002* |
| | 2 | 200 ± 2 | 8397 ± 392* |
| | 3 | 244 ± 6 | 2556 ± 83* |
| A30P | 1 | 921 ± 12 | 8441 ± 319* |
| | 2 | 505 ± 33 | 3297 ± 153* |
| | 3 | 660 ± 15 | 6834 ± 199* |
| E46K | 1 | 254 ± 12 | 1991 ± 304* |
| | 2 | 324 ± 9 | 2938 ± 145* |
| | 3 | 299 ± 7 | 5944 ± 251* |
| A53T | 1 | 216 ± 7 | 2513 ± 102* |
| | 2 | 324 ± 9 | 4076 ± 85* |
| | 3 | 202 ± 12 | 2191 ± 430* |

Note: $\tau_1$ and $\tau_2$ denote the lifetimes of type 1 and type 2 dimers, respectively. *In each case, the lifetime of type 2 dimer is significantly longer than that of type 1, $p < 0.01$.

Table S3. Activation energy barriers for α-Syn dimers

| | WT ($k_BT$) | A30P ($k_BT$) | E46K ($k_BT$) | A53T ($k_BT$) |
|---|---|---|---|---|
| Type-1 | 27.8 ± 0.4 | 29.1 ± 0.6 | 28.2 ± 0.5 | 28.0 ± 0.7 |
| Type-2 | 30.7 ± 1.3 | 31.1 ± 0.8 | 30.7 ± 1.2 | 30.5 ± 1.1 |

## Supplementary movies

Movie S1. Footage of stability of ultra-stable Cy3 covalently immobilized on cover slip

Movie S2. Footage of photobleaching of regular Cy3 covalently immobilized on cover slip

Movie S3. Footage of WT α-Syn dimerization.

Movie S4. Footage of A30P α-Syn dimerization.

Movie S5. Footage of E46K α-Syn dimerization.

Movie S6. Footage of A53T α-Syn dimerization.

## References


1. Krasnoslobodtsev, A. V., J. Peng, J…, Y. L. Lyubchenko. 2012. Effect of spermidine on misfolding and interactions of alpha-synuclein. *PLoS One* 7:e38099.
2. Krasnoslobodtsev, A. V., I. L. Volkov, …, Y. L. Lyubchenko. 2013. alpha-Synuclein Misfolding Assessed with Single Molecule AFM Force Spectroscopy: Effect of Pathogenic Mutations. *Biochemistry* 52:7377-7386.
3. Roy, R., S. Hohng, and T. Ha. 2008. A practical guide to single-molecule FRET. *Nat Methods* 5:507-516.
4. Shlyakhtenko, L. S., J. Gilmore, …, Y. L. Lyubchenko. 2009. Molecular mechanism underlying RAG1/RAG2 synaptic complex formation. *J. Biol. Chem.* 284:20956-20965.